Chemical Science

Accepted Manuscript

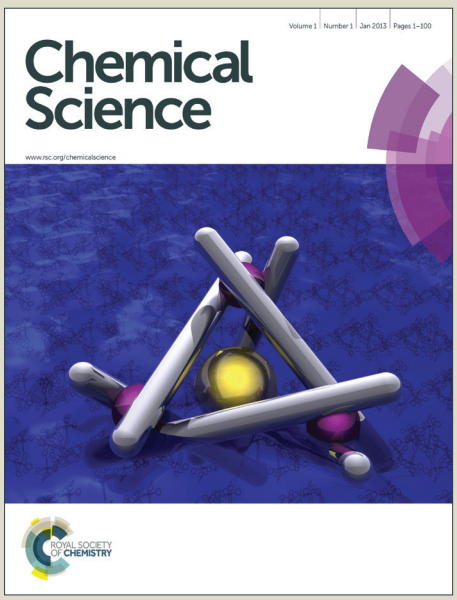

ROYAL SOCIETY OF CHEMISTRY

www.rsc.org/chemicalscience

Journal Name RSCPublishing

ARTICLE

Cite this: DOI: 10.1039/x0xx00000x

Received 00th January 2012,
Accepted 00th January 2012

DOI: 10.1039/x0xx00000x

www.rsc.org/

Unravelling the Correlation between Metal Induced Aggregation and Cellular Uptake/Subcellular Localization of Znsalen: An Overlooked Rule for Design of Luminescent Metal Probes

Juan Tang,[a] Yuan-Bo Cai,[a] Jing Jing[b] and Jun-Long Zhang*[a]

Unravelling the uniqueness of metal coordination on the biological behaviours is of importance to design metal based therapeutic and diagnostic agents. In this work, we chose luminescent Znsalen (**ZnL$_1$**) as a case study to demonstrate that metal induced aggregation arising from intermolecular Zn···O interaction influences its cellular uptake and subcellular localization. Through comparative studies with the free base (**L$_1$** and **L$_2$**), **ZnL$_1$** undergoes cellular uptake through caveolae-mediated endocytosis and internalizes in endosomal/lysosomal compartments, in contrast to the mitochondria where **L$_1$** and **L$_2$** localize. Further studies such as photophysical properties, TEM imaging and DLS analysis suggest that **ZnL$_1$** tends to form large sized fibrous structures in aqueous media. To correlate the relationship between **ZnL$_1$** aggregation and the biological behaviour, we used pyridine to tune the "aggregation-to-deaggregation" transition and found that, in the presence of pyridine, **ZnL$_1$** could localize in mitochondria and internalize into cells through passive diffusion pathway. Such distinctive biological behaviours resulted from different Znsalen species clearly point out the importance of metal induced aggregation in designing metal complexes as biological probes.

Introduction

Luminescent metal complexes have emerged as an important class of imaging agents, for their photophysical properties such as high luminescence, good photostability, large Stokes shifts and long life-times.[1-10] Moreover, metal coordination renders luminescent metal complexes greater flexibility and diversity in structures, compared to organic fluorophores.[6, 7, 11-13] Thus, deciphering the structural rules governing the biological behaviours is of importance to explore the features of luminescent metal complexes in molecular imaging. Despite tremendous progress made in the relationships between structural information arising from coordination such as lipophilicity, oxidation state, charge state and coordination mode, and biological behaviours, much less attention has been given to the physical state or association of luminescent metal complexes in aqueous media.[3, 7, 9, 14] For metal complexes, the intermolecular metal-ligand or metal-metal interactions reinforce the aggregation process, which may influence the mobility of metal complex, and therefore constrain pathways of exposure to cell and affect the subcellular distribution. Thus, the chemical and physical form of a metal complex in aqueous solution might be an important factor in designing luminescent imaging agents. To address this issue, we herein chose Znsalen complex (salen= N,N'-bis(salicylidene)ethylenediamine) as a case study to demonstrate that metal induced aggregation arising from intermolecular Zn···O interaction indeed influences its cellular uptake and subcellular localization.

Znsalens were selected because Zn^{2+} ion possess a high Lewis acidity within planar geometry that allows for an extra coordination of Lewis base ligand or coordinating solvent, or in their absence, self-assembly through intermolecular Zn···O axial coordination to the phenolic group of the other unit.[15-22] Such speciation of Znsalens or salophens is accompanied with changes of morphology and "switched off/on" fluorescence corresponding to "aggregation-to-deaggregation" transition.[15, 21, 23-25] This forms a chemical basis to design optical sensors to detect the anions, biological alkaloids, and even metal cations.[23, 26-30] Extending this prominent feature to living cell imaging, Znsalens could be used as low cytotoxic agents and display high fluorescence in defined organelles, where the environment is more hydrophobic than cytosol or cell culture media.[31-34] Since Znsalen tends to aggregate in aqueous media, it is feasible to investigate whether and how Znsalen aggregation affects the biological behaviours such as cellular uptake and subcellular location. This would be important to further design luminescent Znsalen complexes as bioprobes,[35, 36] combining the insights gained from coordination chemistry of Znsalens.

To demonstrate the effect of Zn coordination on biological behaviours, we performed comparative studies of cell imaging experiments between a water-soluble Znsalen, **ZnL$_1$**, which is conjugated with the mitochondria-targeting triphenylphosphonium cation (TPP), and its free base congener **L$_1$** and **L$_2$** (Scheme 1a).[37-42] Distinctive subcellular distribution between **ZnL$_1$** (lysosomal /endosomal compartments) and free base **L$_1$** and **L$_2$** (mitochondria) indicated the significant biological effect arising from Zn

coordination. Using $\mathbf{L_1}$ and $\mathbf{L_2}$ as controls, we excluded the factors

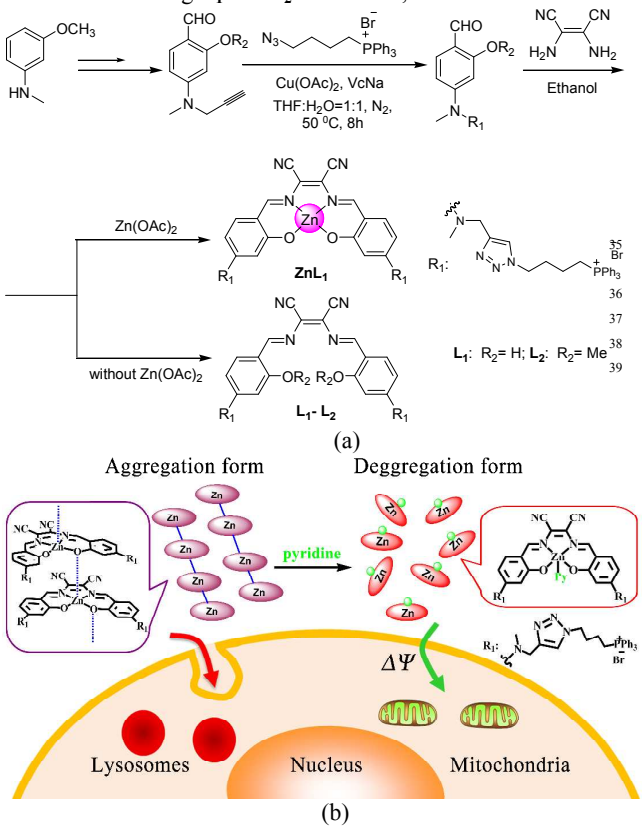

Scheme 1 (a) Synthetic routes and chemical structures of $\mathbf{ZnL_1}$, $\mathbf{L_1}$ and $\mathbf{L_2}$. (b) Aggregation and deaggregation forms of $\mathbf{ZnL_1}$ in aqueous media lead to the different cellular uptake pathways and subcellular localization.

such as lipophilicity and charge state on biological behaviours. Then, we hypothesized intermolecular Zn···O interaction driving $\mathbf{ZnL_1}$ aggregation plays an important role on their distinctive biological behaviours, according to the photophysical properties and morphology of $\mathbf{ZnL_1}$ and $\mathbf{L_1}$ in aqueous media. To confirm this hypothesis, we used pyridine as extra ligand to dissociate aggregates by breaking intermolecular Zn···O interaction and found that $\mathbf{ZnL_1}$ undergoes the passive diffusion pathway and mainly localizes in mitochondria (Scheme 1b). Thus, these results point out the importance of metal induced aggregation to determine biological behaviours, which is potentially useful to design of luminescent metal probes with organelle specificity.

Results and Discussion

$\mathbf{ZnL_1}$ and $\mathbf{L_1}$ were synthesized according to Scheme 1a. N-substituted salicylaldehyde was obtained from 3-methoxyl-N-methylaniline and propargyl bromide, followed by Vilsmeier-Haack formylation. TPP was introduced by copper-catalyzed "Click" reaction. $\mathbf{ZnL_1}$ was synthesized through "one pot" reaction of salicylaldehyde, diimine and zinc acetate, while $\mathbf{L_1}$ was obtained in the absence of zinc acetate. To increase the lipophilicity of $\mathbf{L_1}$, we prepared $\mathbf{L_2}$ as control using methyl group of protected phenol moiety of salicylaldehyde (supporting information). The detailed synthetic procedure and characterization by ^{1}H NMR, ^{13}C NMR, ESI-MS, UV- *vis* and IR were listed in supporting information.

As shown in Fig. 1a, absorption spectra of $\mathbf{ZnL_1}$, $\mathbf{L_1}$ and $\mathbf{L_2}$ in DMSO solution (2×10^{-5} M) show two major absorption bands

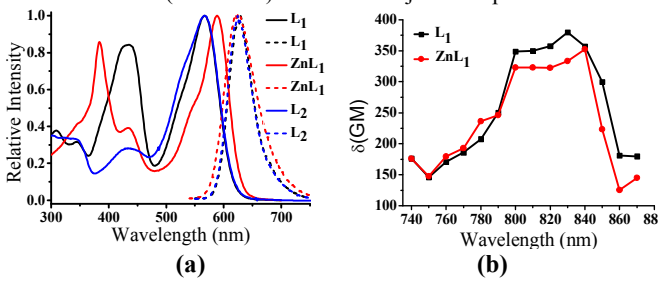

Figure 1. (a) Normalized UV-*vis* and fluorescence spectra of $\mathbf{ZnL_1}$, $\mathbf{L_1}$ and $\mathbf{L_2}$ in DMSO. λ_{ex} = 380 nm. (b) Two photon induced absorption cross-section of $\mathbf{ZnL_1}$ and $\mathbf{L_1}$ in DMSO using Rhodamine B as a reference.

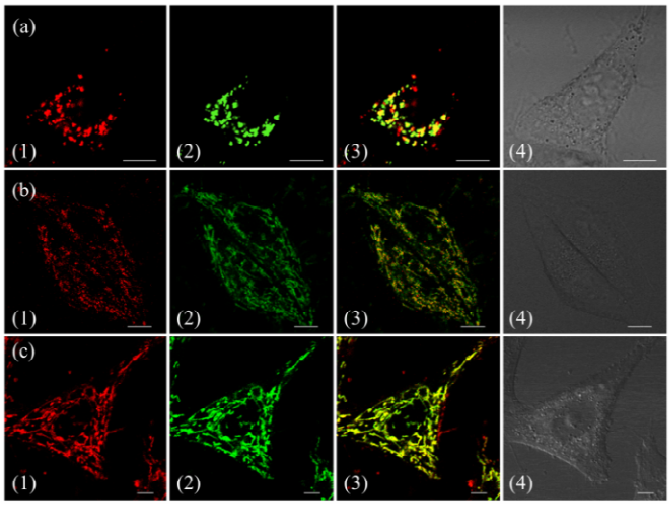

Figure 2. Co-localization analysis of (a) $\mathbf{ZnL_1}$ with lysosome tracker and (b-c) $\mathbf{L_1}$ or $\mathbf{L_2}$ with mitochondria tracker. (1) fluorescence images of $\mathbf{ZnL_1}$, $\mathbf{L_1}$ and $\mathbf{L_2}$, ex: 543 nm; (2) fluorescence images of commercial trackers including LysoTracker® Green DND-26 in (a) or MitoTracker Green in (b-c), ex: 488 nm; (3) merged images of (1) and (2); (4) differential interference contrast channel. Scale bar: 10 μm.

between 350-450 and 500-600 nm, respectively. Free bases $\mathbf{L_1}$ and $\mathbf{L_2}$ display a broad absorption bands from 360 to 470 nm, whereas $\mathbf{ZnL_1}$ shows a sharp band centered at 385 nm with a low-energy shoulder at 435 nm. Low-energy bands are likely due to internal charge transfer (ICT) transition. $\mathbf{ZnL_1}$, $\mathbf{L_1}$ and $\mathbf{L_2}$ exhibit red emission (λ_{max} = 623, 631 and 624 nm for $\mathbf{ZnL_1}$, $\mathbf{L_1}$ and $\mathbf{L_2}$ in DMSO, respectively) with the fluorescence quantum yields of 0.26, 0.29 and 0.21 (Table S1). ^{1}H NMR spectra of $\mathbf{ZnL_1}$, $\mathbf{L_1}$ and $\mathbf{L_2}$ in d^6-DMSO displays sharp signals with the expected multiplicity according to their molecular structures (Fig. S15-17). Following Di Bella's procedure, we used diffusion-ordered spectroscopy (DOSY) NMR to estimate the molecular weight of $\mathbf{ZnL_1}$ in d^6-DMSO (Table S4, Fig. S18). The obtained molecular weight is *ca.*1260, close to that of calculated molecular weight. These results clearly suggest monomeric $\mathbf{ZnL_1}$ is the main specie in coordinating solvent DMSO. In addition, the lipophilicity of $\mathbf{ZnL_1}$, $\mathbf{L_1}$ and $\mathbf{L_2}$ were measured by the logarithm of octanol/water partition coefficients (log *Ps* 0.12, -0.77, 0.09) according to Leo's method.[43] This suggests that Zn coordination increase the lipophilicity of $\mathbf{L_1}$, which is comparable to methoxylation of phenolic group of $\mathbf{L_1}$ (Table S2).

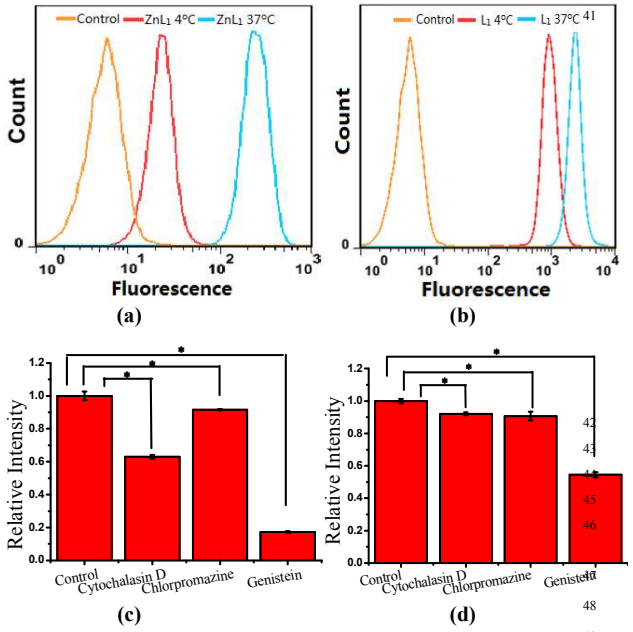

Figure 3. Cellular uptake of **ZnL$_1$** and **L$_1$** analyzed by flow cytometry. Internalization of **ZnL$_1$** (a) or **L$_1$**(b) was investigated at 4 and 37 °C. Cells treated with HeLa cells were treated with cytochalasin D (5 μg·mL^{-1}), chlorpromazine (10 μg·mL^{-1}) and genistein (100 μM) for 30 min and then incubated with inhibitor and **ZnL$_1$** or **L$_1$** (2 μM) for 1 h. Cells treated with **ZnL$_1$** or **L$_1$** only were treated as controls. Mean relative intracellular fluorescence intensities of intracellular uptake of **ZnL$_1$** (c) and L$_1$ (d) were shown in histograms (n=3, *P < 0.001).

Zn coordination affects cellular uptake and subcellular distribution

To demonstrate the effect of Zn coordination on biological behaviours, we investigated the intracellular distribution of **ZnL$_1$**, **L$_1$** and **L$_2$** in HeLa cells using confocal laser scanning microscopy. FYVE-EGFP, EHD1-EGFP, LysoTracker® Green DND-26, MitoTracker Green served as markers for organelles early endosome and late endosome, lysosome and mitochondria, respectively. As shown in Fig. 2a and S1-2, **ZnL$_1$** showed good cell permeability and mainly distributed in lysosomal/endosomal compartments. It exhibited a co-localization level of approximately 0.56 with LysoTracker® Green DND-26. Interestingly, **L$_1$** and **L$_2$** particularly stained mitochondria with Pearson's correlation coefficients of 0.92 and 0.83 (Fig. 2b, c). Similar subcellular distributions of **L$_1$** and **L$_2$** clearly suggested that the lipophicility of salen ligands is not the main factor to affect subcellular distribution.

To explore the effect of Zn coordination on cellular uptake pathway, temperature-dependent cellular uptake of **ZnL$_1$** or **L$_1$** with HeLa cells was carried out at 4 and 37ºC analysed by flow cytometry. As shown in Fig. 3a-b, cellular internalization of **ZnL$_1$** at 4ºC showed significantly lower intracellular level compared to cells incubated in parallel at 37ºC, whereas **L$_1$** is less affected by temperature. This indicates that cellular internalization of **ZnL$_1$** is an active process despite of the low intracellular luminescence in cells incubated at 4ºC. In contrast, passive diffusion might be the dominant mechanism for the free base **L$_1$**, although a background level of active transport also occurs.

To demonstrate the cellular internalization of **ZnL$_1$**, we then used flow cytometry by applying various endocytosis inhibitors including chlorpromazine (inhibitor of clathrin-mediated endocytosis)[44-46]; genistein (inhibitor of caveolae-mediated endocytosis) [44, 47, 48], cytochalasin D (inhibitor of macropinocytosis)[49-53]. As Fig. 3c-d showed, the treatment with 100 μg·mL^{-1} genisteins resulted in drastic decrease of 80% in the cellular uptake of **ZnL$_1$**, suggesting that **ZnL$_1$** is mainly internalized via caveolae-mediated endocytosis, which plays a general role for the internalization of large sized particles into cells.[52, 54, 55] In addition, treatment with cytochalasin D also led to 40% decrease in cellular uptake, suggesting that macropinocytosis-mediated pathway might also partly involved (Fig. 3c). In contrast, for **L$_1$**, the treatment of genisteins only resulted in 45% decrease in the cellular uptake, and no obvious influence was observed when treated with cytochalasin D or chlorpromazine, which indicates that **L$_1$** partly undergoes caveolae-mediated endocytosis and may mainly cross cell membrane by passive transport, and then internalizes to mitochondria (Fig. 3d). Furthermore, to exclude the possibility that zinc coordination diminish the mitochondrial permeation capability, we examined the ability of **ZnL$_1$** and **L$_1$** to stain the isolated mitochondria. Following Schagger's procedure,[56] we isolated mitochondrial fractions and confirmed the activity by JC-1, shown in Fig. S4. After incubation of **ZnL$_1$** and **L$_1$** with active mitochondria for 0.5 h, the fluorescence of resuspended mitochondria was detected (Fig. S11), indicating the mitochondrial permeation capability of **ZnL$_1$** and **L$_1$**. To further verify this, we also used giant unilamellar phospholipid vesicles (GUVs) as mitochondria models following Pielak's method (Fig. S6).[57] As shown in Fig. 4, both **ZnL$_1$** and **L$_1$** permeated into mitochondria mimic membranes and localized in GUVs matrix after 20 min. These results suggested that Zn coordination does not affect mitochondria permeating capability, and different subcellular distributions of **ZnL$_1$** and **L$_1$** might be due to cellular uptake pathways.

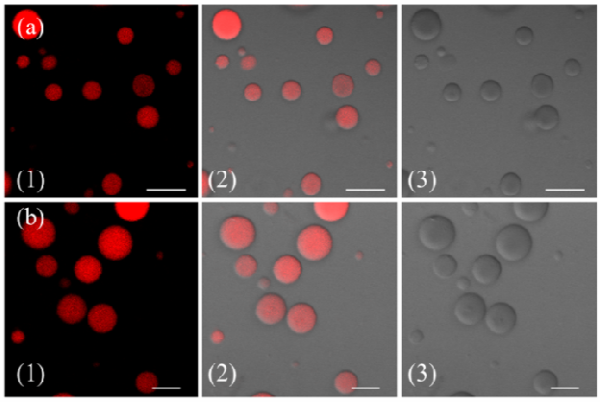

Figure 4. Mitochondria permeability investigation of **ZnL$_1$** and **L$_1$**.with GUVs mimics Confocal images of (a) **ZnL$_1$** and (b) **L$_1$** confined in GUVs. (a) fluorescence images of **ZnL$_1$** and **L$_1$**; (2) merged images of (1) and (3); and (3) differential interference contrast channel. Scale bar: 10 μm.

Photophysical properties and morphology in aqueous media

Since cellular uptake of **ZnL$_1$** is related to caveolae-mediated endocytosis and macropinocytosis, we envisioned that the behaviour of **ZnL$_1$** in aqueous media might influence the cellular uptake and subcellular distribution. To understand it, we carried out UV-*vis* absorption and emission spectra of **ZnL$_1$** and **L$_1$** (Figs. 5b-c, S7-8) in aqueous media. Increasing water content to DMSO solution, both **ZnL$_1$** and **L$_1$** display blue shifts of 15 nm

Journal Name RSCPublishing

ARTICLE

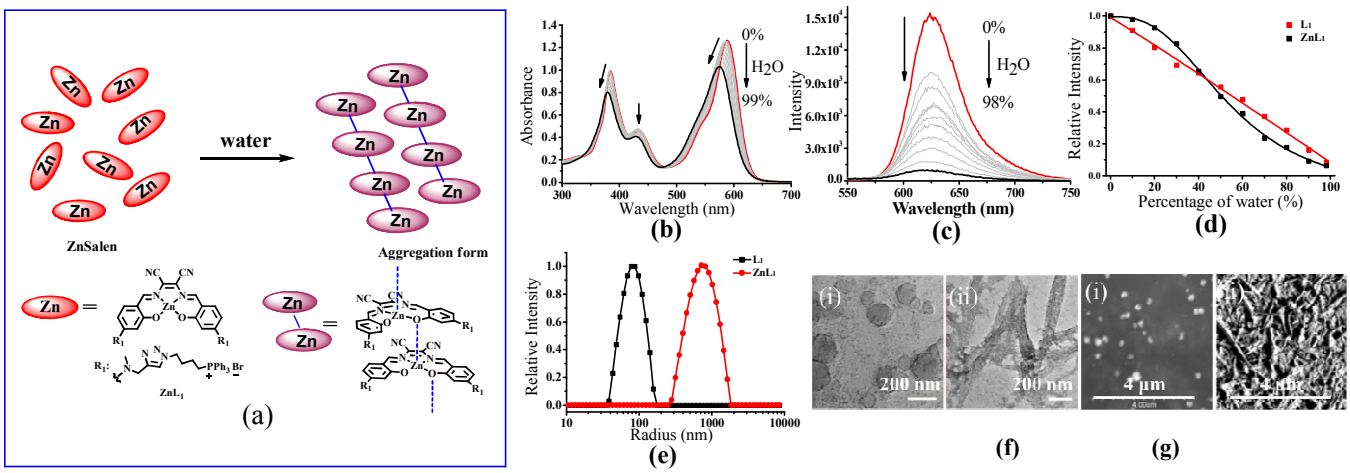

Figure 5. (a) The change of speciation of **ZnL$_1$** in water solution. (b) UV-*vis* and (c) fluorescence spectra (λ_{ex} = 380 nm) of **ZnL$_1$** (20 μM) in the mixed solution of H_2O/DMSO. The content of H_2O was from 0% to 99%. (d) Fluorescence changes of **ZnL$_1$** and **L$_1$** along with different percentage of water. (e) DLS analysis of **ZnL$_1$** and **L$_1$** in water containing 0.1% DMSO. (f) TEM images of self-assembled (i) **L$_1$** and (ii) **ZnL$_1$** (scale bar: 200 nm). (g) SEM pictures of two assemblies of (i) **L$_1$** and (ii) **ZnL$_1$** (scale bar: 4 μm).

and 26 nm for low-energy absorption, and the emission is quenched gradually with blue shifts of 6 and 11 nm,respectively. No clear isosbestic point in absorption spectra and quenched fluorescence for **ZnL$_1$** and **L$_1$** suggested the formation of aggregates in aqueous media.[58, 59, 19, 60] Interestingly, plotting the emission intensity of **ZnL$_1$** and **L$_1$** versus water contents (%) showed the logistic regression with P values of 2.71 and 1.04(Fig. 5d). Larger P value for **ZnL$_1$** indicated cooperative effect on the formation **ZnL$_1$** aggregates in aqueous media.

^{1}H NMR spectra of **ZnL$_1$** and **L$_1$** (concentration: 1 mM) in the mixtures of D_2O and d^6-DMSO solvents (Fig. S11) shows the protons of salen skeleton became broaden and the intensity decreased progressively with the increasing contents of D_2O, which is probably due to restricted motion of hydrophobic salen moiety whereas the signals of triphenylphosphonium group did not significantly change. In addition, diffusion-ordered spectroscopy (DOSY) NMR for ZnL1 in d^6-DMSO solution containing 30% D_2O showed the average molecular mass of 1602 (Table S4, Fig. S19), indicating partly aggregation of ZnL1 under this condition. However, for the broad and weak signals, we cannot obtain the reliable DOSY data in higher concentration of D_2O, which are predicted to form larger aggregates. Nevertheless, optical spectroscopy data and NMR spectroscopic studies clearly indicate the "deaggregation to aggregation" transition of **ZnL$_1$** when the solvent was switched from DMSO to water.

To further examine the morphology of **ZnL$_1$** or **L$_1$** in aqueous media, dynamic light scattering (DLS) experiments were performed. As shown in Fig. 5e, **L$_1$** (1 μM) has a smaller hydrodynamic diameter (Dr, *ca.* 60 nm) and narrower distribution than **ZnL$_1$** (Dr, *ca.* 720 nm). No change of **ZnL$_1$** or **L$_1$** aggregates were observed in cell culture media (Fig. S9), indicating the intergradient in cell culture media has little effect on the aggregates. Then, the morphology of **ZnL$_1$** and **L$_1$** aggregates was studied by transmission electron microscopy (TEM) and scanning electron microscope (SEM) by drop-casting the aqueous solutions of **ZnL$_1$** or **L$_1$** onto Cu-C (200) substrates. As shown in Fig. 5f-g, TEM and SEM images clearly show the formation of a fibrous nanostructure (a dimension of 43.5±2.6 nm and more than 1 μm in length) for **ZnL$_1$**, while **L$_1$** shows a distinct globular morphology with a dimension range from 20 nm to 70 nm, which are consistent to the DLS results. To exclude the effect of lipophilicity, we used **L$_2$** as control and **L$_2$** exhibited similar particle size and distribution to those of **L$_1$** in both aqueous solution and cell culture medium (Fig. S9-10). Given the similar structure of **ZnL$_1$**, **L$_1$** and **L$_2$**, we ascribed the different morphologies in aqueous media is due to intermolecular Zn···O interaction between **ZnL$_1$** aggregates (Scheme 1b).

Although the aggregation of Znsalen complexes through intermolecular Zn···O interaction in non-coordinating solvents is a usual feature, such studies in water have much less been reported. There are several examples of water soluble Znsalens found to be monomeric species in aqueous solutions,[27, 28, 61] thus water effect on the aggregation of **ZnL$_1$** in water needs further discussed. Generally, water is a Lewis base and coordinating solvent and can compete with intermolecular Zn···O interactions and hence may prevent aggregation. However, another facet of water as solvent, in which the hydrophobic effect of Znsalen promotes such aggregation,

Journal Name RSCPublishing

ARTICLE

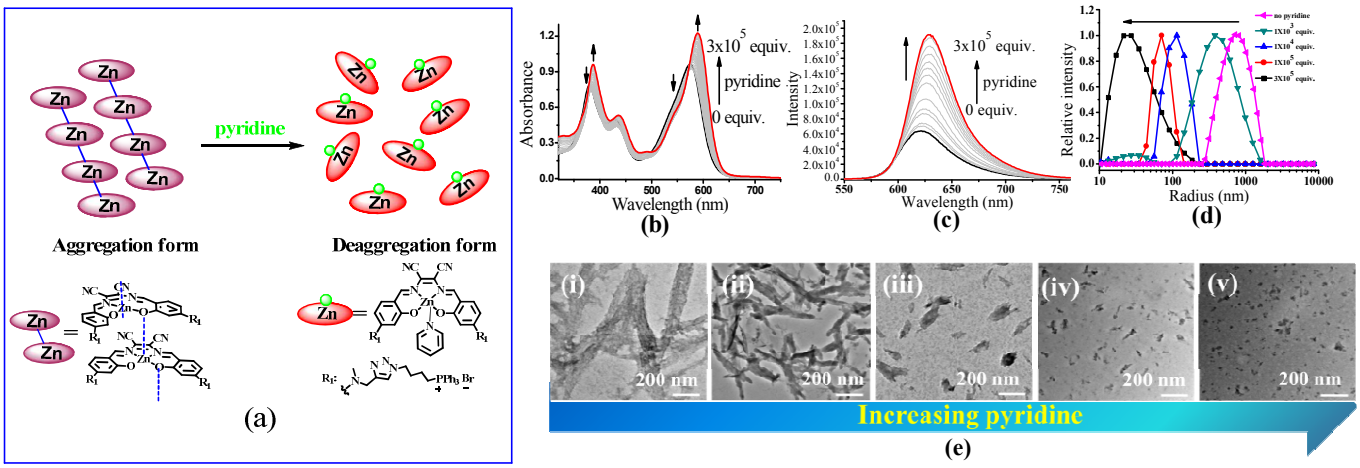

Figure 6. (a) The change of speciation of $\mathbf{ZnL_1}$ in the presence of pyridine. The dissociation of the aggregated state of 20 μM $\mathbf{ZnL_1}$ induced by competitive pyridine binding monitored by (b) UV-*vis* and (c) fluorescence spectra. (d) DLS analysis of $\mathbf{ZnL_1}$ (1 μM) in water.and adding 0-300 thousands equiv. pyridine. (e) TEM images of self-assembled $\mathbf{ZnL_1}$ in the presence of (i-v) 0, 1×10^3, 1×10^4, 1×10^5, 3×10^5 equiv. pyridine. Scale bar is 200 nm.

cannot be neglected. Obviously, the roles of water are complicate, which is highly dependent on the different binding affinities of H_2O-Zn and intermolecular phenolic O-Zn interaction, the structures and lipophilicity of Znsalen, the properties of conjugates and solvent effect. In this work, the formation of $\mathbf{ZnL_1}$ aggregates in water confirmed by UV-*vis* absorption, fluorescence and NMR spectroscopic studies together with morphological studies clearly indicates intermolecular Zn···O interaction is more prominent than water coordination. On the other hand, lipophilic triphenylphosphonium cations were introduced, $\mathbf{ZnL_1}$ is to some extent hydrophobic (Log *P* 0.12). The flexible spacer (C4 chain and triazole linker) promotes the aggregation of Znsalen moiety and the triphenylphosphonium cations as head groups locates in the interfaces, which is according to the changes of proton signals in ^{1}H-NMR. Thus, the hydrophobic effect is another important factor to determine $\mathbf{ZnL_1}$ aggregation in water.

Stability of $\mathbf{ZnL_1}$ aggregates in aqueous media

To understand the contribution of intermolecular Zn···O interaction to $\mathbf{ZnL_1}$ aggregation, we carried out competitive pyridine binding experiments. According to previous studies,[15, 17-19] competitive Lewis bases such as pyridine binding would dissociate the aggregates if intermolecular Zn···O interaction was the main driving force for the self-assembly process in non-coordination solvents. Asshown in Fig. 6b, when pyridine was added to aqueous solution of $\mathbf{ZnL_1}$, the bands at around 380 and 550 nm red shifted to 387 and 590 nm, indicating the dissociation of $\mathbf{ZnL_1}$ aggregates. As expected, fluorescence intensity increases along with the increasing amount of pyridine (Fig. 6c). Fluorescence lifetimes were recorded before and after pyridine addition. In water, the luminescence decays are fitted as double-exponential decays with lifetimes 2.0 (76%) and 5.2 (24%) ns. After pyridine titration, fluorescence lifetime is 4.0 ns with single-exponential decay, slightly shorter than that in DMSO (5.2 ns). Complete deaggregation of $\mathbf{ZnL_1}$ needs up to 2×10^5 equiv. pyridine (Fig. S12), which is comparable to the extremely stable bimetallic Znsalen complex reported by Kleij and coworkers.[20] Monitoring pyridine titration in ^{1}H NMR spectra demonstrated the sharpen proton signals of $\mathbf{ZnL_1}$ with downfield shifts (Fig. S13), also supporting the deaggregation of $\mathbf{ZnL_1}$ by pyridine. Moreover, the dissociation of $\mathbf{ZnL_1}$ aggregates is evident from DLS results and TEM imaging. Fig. 6d showed the decreased hydrodynamic radius from 720 nm to 27 nm along with increasing 0 to 300 thousands equiv. pyridine. TEM imaging confirmed this trend and showed the size of aggregates reduced from 1250±117 to 31±2.3 nm (Fig. 6e).

Besides pyridine, we attempted to test anion effect on $\mathbf{ZnL_1}$ aggregation in aqueous media. Previous studies demonstrated that anions such as phosphate,[23, 27, 61] Br^- [25] are able to coordinate Zn and dissociate Znsalen aggregation, however, with much smaller binding constants than pyridine.[61, 62] In this work, we chose PO_4^{3-} (PBS buffer), Br^- ($^nBu_4NBr$) and HBSS buffer (containing various inorganic anions), related to biological study. As shown in Fig. 7a-c, increasing the concentrations of PBS, $^nBu_4NBr$ and HBSS from 0 to 50 mM, UV-*vis* spectra showed increasing bandwidths and blue-shifted with decreasing intensity at 500-600 nm, indicating more aggregates formation. To understand this, we proposed that high concentration of anions promoting $\mathbf{ZnL_1}$ aggregation is due to salt effect arising from PBS, $^nBu_4NBr$ and HBSS. To test it, we measured UV-*vis* spectra of $\mathbf{ZnL_1}$ in presence of NaCl (0-49 mM).As shown in Fig. 7d, similar spectroscopic changes were

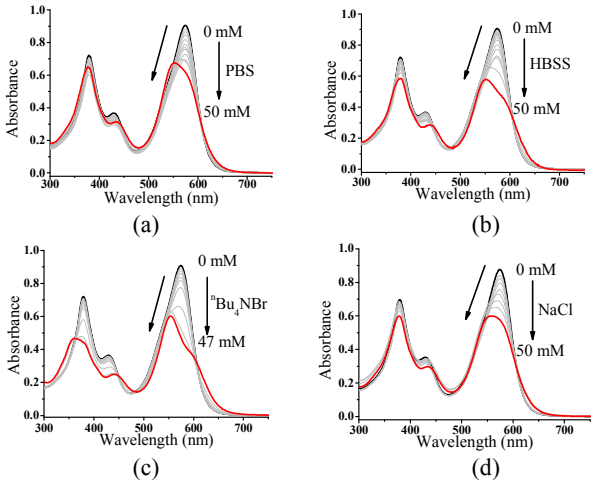

Figure 7. UV-*vis* spectra of 20 μM **ZnL$_1$** in the presence of (a) 0-50 mM PBS, (b) HBSS, (c) $^{n}Bu_4NBr$, and (d) NaCl.

observed. Thus, we concluded that the aggregation of **ZnL$_1$** might be affected by ionic strength from these salts. This also could be used to explain why pyridine is much effective to disassociate **ZnL$_1$**. Excepted for higher binding constant to Zn ion, pyridine is a neutral molecule and the effect of ionic strength could be neglected. Although the "aggregation-to-deaggregation" process for Znsalen/salophens had been extensively studied,[15, 18-21] few studies for the stability of such aggregates in aqueous media was performed. This is important to verify whether the aggregates are stable enough to affect the biological behaviours. Following Kleij's method,[18, 20] we also estimate the stability constants of **ZnL$_1$** aggregates in aqueous media. Relationship of overall aggregation constant K_{agg}, stepwise aggregation constant $K_{n/n+1}$, and the aggregation number n can be described as the following equation:

$$(ZnSalen)_n + nPy \rightleftharpoons n\ ZnSalen(Py) \quad K=K_{py}^{n}/K_{agg},\ K_{agg}=K_{n/n+1}^{n-1} \qquad (1)$$

In this equation, K_{py} represents the coordination constant of pyridine to Zn center of **ZnL$_1$**. To evaluate K_{py}, we carried out pyridine titration to the solution of **ZnL$_1$** in dichloromethane (DCM) (Fig. S14). The coordination constant was calculated to be 1.4×10^4 M^{-1}, which is lower than those (5.3 and 5.9×10^5) reported by Kleij,[18, 26] and 4.7×10^6 reported by Di Bella.[62] The lower coordination constant was probably due to the interference of the large triphenylphosphnium groups. As to the pyridine titration in aqueous solution, the increase at 590 nm was monitored to calculate the total reaction constant K. K_{agg} and $K_{n/n+1}$ depending on aggregation number n. Table S3 lists all the calculated K_{agg} and $K_{n/n+1}$ with increasing aggregation numbers. Each addition of monomer to a previously formed oligomer has a high association constant in the order of about 10^{10} M^{-1}, which is even about 2 orders higher than dimerization of Znsalens in organic solvents.[18] This clearly demonstrates solvent effect reinforces intermolecular Zn···O interaction and enhances the stability of **ZnL$_1$** aggregates.

Effect of the "aggregation/deaggregation" process on the biological behaviours

To confirm the hypothesis that **ZnL$_1$** aggregation affected the biological behaviours, we performed cell imaging experiments using

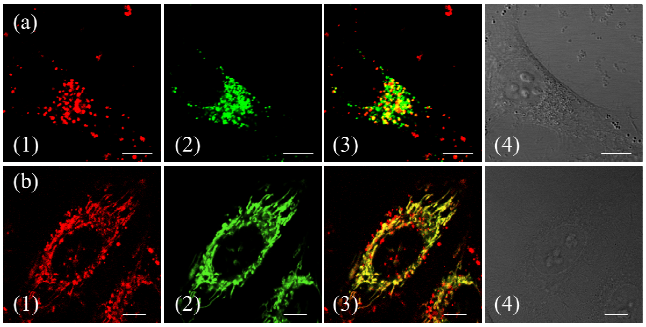

Figure 8. Co-localization analysis of (a) **ZnL$_1$** in absence of pyridine with lysosomes and (b) **ZnL$_1$** in presence of pyridine with mitochondria: (1) fluorescence images of **ZnL$_1$**, ex=543 nm; (2) fluorescence of commercial trackers including LysoTracker® Green DND-26 in (a) or MitoTracker Green in (b), ex=488 nm; (c) merged picture of (1) and (2); (4) differential interference contrast channel. Scale bar: 10 μm.

ZnL$_1$ in the presence or absence of pyridine. According to the above results, **ZnL$_1$** aggregates can be dissociated by the addition of pyridine, which would exhibit different cellular uptake pathways and subcellular distributions from the sole use of **ZnL$_1$**. The intracellular luminescence and subcellular distribution of **ZnL$_1$** were investigated in HeLa cells by confocal laser scanning microscopy (CLSM). As shown in Fig. 8a, in the absence of pyridine, **ZnL$_1$** exhibited punctuate red fluorescence in lysosomal/endosomal compartments, which mainly co-localized with the LysoTracker® Green DND-26 (Pearson's correlation coefficient 0.56). In contrast, in the presence of pyridine (about 6000 equiv.), **ZnL$_1$** mainly localized in mitochondria and co-localized with the commercial MitoTracker Green (Pearson's correlation coefficient 0.60) (Fig. 8b). These results clearly demonstrate that "aggregation/deaggregation" transition influences subcellular distribution.

To understand whether deaggregation of **ZnL$_1$** in aqueous solution influences the internalization mechanism, we examined temperature dependent cellular uptake using flow cytometry. As shown in Fig. 9a, significantly lower intracellular fluorescence intensity was observed for **ZnL$_1$** in the presence or absence of pyridine at 4 ºC than that at 37 ºC, indicating **ZnL$_1$** species were internalized by cells via a temperature-dependent process. Then, we employed various endocytosis inhibitors including chlorpromazine (inhibitor of clathrin-mediated endocytosis)[44-46], genistein (inhibitor of caveolae-mediated endocytosis)[44, 47, 48], cytochalasin D (inhibitor of macropinocytosis)[49-53] as mentioned above, to investigate whether **ZnL$_1$** internalizes into cell through endocytosis. As shown in Fig. 9b, in the presence of pyridine, the treatments with genistein, cytochalasin D or chlorpromazine only resulted in a moderate decrease of intracellular fluorescence (27%, 17% and 14%, respectively) and thus cellular uptake of **ZnL$_1$** in the presence of pyridine is almost not correlated to endocytosis, which is markedly different from the endocytosis pathway of **ZnL$_1$** in aggregation state.

Given TPP conjugate possesses positive charge, internalization of **ZnL$_1$** with pyridine may be facilitated by organic cation transporter (OCT) or driven by the plasma membrane potential (-50 to -70 mV, negative inside).[63-66] When using tetrabutylammonium bromide as the OCT inhibitor[67], HeLa cells showed no obvious intracellular fluorescence change (Fig. 9c-d). To investigate the effect of plasma membrane potential, we examined cellular uptake of **ZnL$_1$** in the

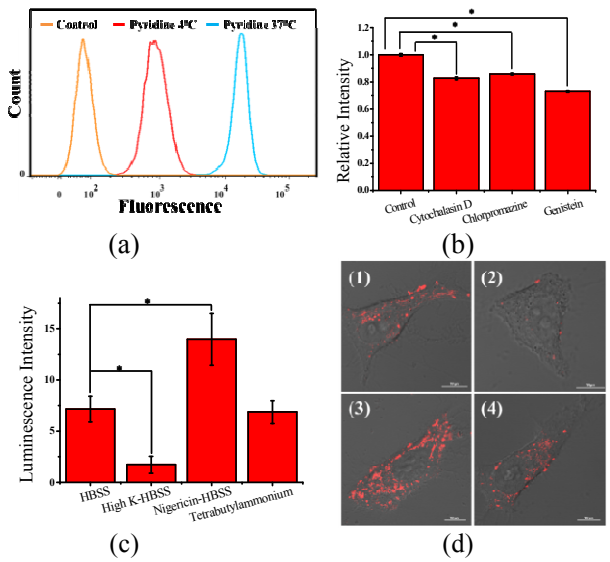

Figure 9. Cellular uptake of $\mathbf{ZnL_1}$ analysed by flow cytometry and CLSM. (a) Effect of incubation temperature on internalization of $\mathbf{ZnL_1}$ in presence of pyridine was investigated at 4 and 37 °C. (b) Effect of endocytosis on internalization of $\mathbf{ZnL_1}$ in presence of pyridine: HeLa cells were treated with cytochalasin D (5 μg•mL^{-1}), chlorpromazine (10 μg•mL^{-1}) and genistein (100 μM) for 30 min and then incubated with inhibitor and $\mathbf{ZnL_1}$ (2 μM) for 1 h. Cells treated with $\mathbf{ZnL_1}$ only were treated as controls. (c) and (d) Effect of the plasma membrane potential and organic cation transporter inhibitor on internalization of $\mathbf{ZnL_1}$: HeLa cells treated with $\mathbf{ZnL_1}$ in presence of pyridine buffered in (1) HBSS, (2) high K^+-HBSS, (3) 5 μM nigericin-HBSS (Cells were treated with 5 μM nigericin first for 30 min) or (4) 1 mM tetrabutylammonium bromide-HBSS (Cells were treated with 1 mM tetrabutylammonium bromide first for 20 min). Mean relative intracellular fluorescence intensities of intracellular uptake were shown in histograms (n = 3, *P < 0.001). Scale bar: 10 μm.

presence of pyridine under the conditions such as high potassium buffer (K^+-HBSS, 170 mM K^+, depolarization) [65, 67, 68] and nigericin-HBSS (10 μM, hyperpolarization) [65, 69]. As shown in Fig. 9c-d, K^+-HBSS- treated cells displayed a remarkable decrease of intracellular fluorescence (80%), while nigericin-treated cells showed intracellular fluorescence increases to 2 fold. This clearly demonstrated that $\mathbf{ZnL_1}$ in the presence of pyridine is internalized mostly by the membrane potential dependent passive diffusion. Since we have demonstrated that PBS, HBSS, and Br^- cannot lead to $\mathbf{ZnL_1}$ deaggregation and couldn't disturb pyridine coordination, combining with photophysical properties and morphology in aqueous media, we hypothesized the distinctive internalization pathways may be due to different morphologies between the "aggregation/deaggregation" transition of $\mathbf{ZnL_1}$, because the caveolae-mediated or macropinocytosis-mediated endocytosis is related to uptake of large sized particles into cells.[44, 66, 68]

Conclusions

Taken together, we demonstrated that intermolecular Zn···O interaction between Znsalen played an important role to determine its cellular uptake pathway and subcellular distribution. Through comparative studies between $\mathbf{ZnL_1}$ and free bases $\mathbf{L_1}$ and $\mathbf{L_2}$, Zn coordination leads to distinctive cellular uptake pathway and subcellular distribution. More importantly, the photophysical and morphology studies for $\mathbf{ZnL_1}$ and free bases in aqueous media suggest the different aggregation arising from intermolecular Zn···O interaction play a critical role to influence the biological behaviours. This hypothesis was confirmed by cell imaging experiments using $\mathbf{ZnL_1}$ in the presence or absence of pyridine, which clearly demonstrates cellular uptake pathway and subcellular distribution by tuning "aggregation/deaggregation" transition of $\mathbf{ZnL_1}$ in aqueous media. These results point to a new factor, "metal induced aggregation", is effective to influences cellular uptake and subcellular distribution and should not be overlooked in designing luminescent metal complexes as biological probes.

Acknowledgements

This project was supported by the National Scientific Foundation of China and National Key Basic Research Support Foundation of China (NKBRSFC) (2013CB933402, 2015CB856300).

Notes and references

[a] Beijing National Laboratory for Molecular Sciences, State Key Laboratory of Rare Earth Materials Chemistry and Applications, College of Chemistry and Molecular Engineering, Peking University, Beijing 100871, P.R. China, Fax: +86-10-62767034, E-mail: zhangjunlong@pku.edu.cn.
[b] School of Chemistry, Beijing Institute of Technology, Beijing 100081, P.R. China.

† . Electronic Supplementary Information (ESI) available: [details of any supplementary information available should be included here]. See DOI: 10.1039/b000000x/

1. K. L. Haas and K. J. Franz, *Chem. Rev.*, 2009, **109**, 4921-4960.
2. Q. Zhao, C. Huang and F. Li, *Chem. Soc. Rev.*, 2011, **40**, 2508-2524.
3. E. Baggaley, J. A. Weinstein and J. Williams, *Coord. Chem. Rev.*, 2012, **256**, 1762-1785.
4. M. Schäferling, *Angew. Chem. Int. Ed.*, 2012, **51**, 3532-3554.
5. D.-L. Ma, V. P.-Y. Ma, D. S.-H. Chan, K.-H. Leung, H.-Z. He and C.-H. Leung, *Coord. Chem. Rev.*, 2012, **256**, 3087-3113.
6. D. L. Ma, H. Z. He, K. H. Leung, D. S. H. Chan and C. H. Leung, *Angew. Chem. Int. Ed.*, 2013, **52**, 7666-7682.
7. K. K.-W. Lo, A. W.-T. Choi and W. H.-T. Law, *Dalton Trans.*, 2012, **41**, 6021-6047.
8. V. Fernández-Moreira, F. L. Thorp-Greenwood and M. P. Coogan, *Chem. Commun.*, 2010, **46**, 186-202.
9. F. L. Thorp-Greenwood, R. G. Balasingham and M. P. Coogan, *J. Organomet. Chem.*, 2012, **714**, 12-21.
10. D.-L. Ma, D. S.-H. Chan and C.-H. Leung, *Acc. Chem. Res.*, 2014, **47**, 3614-3631.
11. Z. Guo and P. J. Sadler, *Angew. Chem. Int. Ed.*, 1999, **38**, 1512-1531.
12. E. Meggers, *Chem. Commun.*, 2009, **9**, 1001-1010.
13. M. Frezza, S. Hindo, D. Chen, A. Davenport, S. Schmitt, D. Tomco and Q. P. Dou, *Curr. Pharm. Des.*, 2010, **16**, 1813-1825.
14. R. P. Haugland, *The handbook: a guide to fluorescent probes and labeling technologies*, Molecular probes, 2005.
15. C. T. L. Ma and M. J. MacLachlan, *Angew. Chem. Int. Ed.*, 2005, **44**, 4178-4182.
16. J. K. H. Hui, Z. Yu and M. J. MacLachlan, *Angew. Chem. Int. Ed.*, 2007, **46**, 7980-7983.
17. A. W. Kleij, *Dalton Trans.*, 2009, **24**, 4635-4639.
18. M. M. Belmonte, S. J. Wezenberg, R. M. Haak, D. Anselmo, E. C. Escudero-Adan, J. Benet-Buchholz and A. W. Kleij, *Dalton Trans.*, 2010, **39**, 4541-4550.

19. G. Consiglio, S. Failla, P. Finocchiaro, I. P. Oliveri, R. Purrello and S. Di Bella, *Inorg. Chem.*, 2010, **49**, 5134-5142.
20. G. Salassa, M. J. J. Coenen, S. J. Wezenberg, B. L. M. Hendriksen, S. Speller, J. A. A. W. Elemans and A. W. Kleij, *J. Am. Chem. Soc.*, 2012, **134**, 7186-7192.
21. G. Consiglio, S. Failla, P. Finocchiaro, I. P. Oliveri and S. Di Bella, *Inorg. Chem.*, 2012, **51**, 8409-8418.
22. I. P. Oliveri, S. Failla, G. Malandrino and S. Di Bella, *J. Phys. Chem. C*, 2013, **117**, 15335-15341.
23. M. Cano, L. Rodríguez, J. C. Lima, F. Pina, A. Dalla Cort, C. Pasquini and L. Schiaffino, *Inorg. Chem.*, 2009, **48**, 6229-6235.
24. I. P. Oliveri and S. Di Bella, *J. Phys. Chem. A*, 2011, **115**, 14325-14330.
25. I. P. Oliveri, G. Malandrino and S. Di Bella, *Dalton Trans.*, 2014, **43**, 10208-10214.
26. E. C. Escudero-Adán, J. Benet-Buchholz and A. W. Kleij, *Inorg. Chem.*, 2008, **47**, 4256-4263.
27. S. Khatua, S. H. Choi, J. Lee, K. Kim, Y. Do and D. G. Churchill, *Inorg. Chem.*, 2009, **48**, 2993-2999.
28. A. Dalla Cort, P. De Bernardin and L. Schiaffino, *Chirality*, 2009, **21**, 104-109.
29. S. J. Wezenberg, D. Anselmo, E. C. Escudero-Adán, J. Benet-Buchholz and A. W. Kleij, *Eur. J. Inorg. Chem.*, 2010, **29**, 4611-4616.
30. Y.-B. Cai, J. Zhan, Y. Hai and J.-L. Zhang, *Chem. Eur. J.*, 2012, **18**, 4242-4249.
31. J. Jing, J. Tang, D. Xie , Y.-B. Cai, J.-J. Chen and J.-L. Zhang, *Scientia Sinica Chimica*, 2014, **44**, 191-203.
32. Y. Hai, J.-J. Chen, P. Zhao, H. Lv, Y. Yu, P. Xu and J.-L. Zhang, *Chem. Commun.*, 2011, **47**, 2435-2437.
33. J. Jing, J.-J. Chen, Y. Hai, J. Zhan, P. Xu and J.-L. Zhang, *Chem. Sci.*, 2012, **3**, 3315-3320.
34. D. Xie, J. Jing, Y.-B. Cai, J. Tang, J.-J. Chen and J.-L. Zhang, *Chem. Sci.*, 2014, **5**, 2318-2327.
35. J.-J. Chen, J. Jing, H. Chang, Y. Rong, Y. Hai, J. Tang, J.-L. Zhang and P. Xu, *Autophagy*, 2013, **9**, 894-904.
36. J. Jing and J.-L. Zhang, *Chem. Sci.*, 2013, **4**, 2947-2952.
37. R. A. J. Smith, C. M. Porteous, A. M. Gane and M. P. Murphy, *Proc. Natl. Acad. Sci. U. S. A.*, 2003, **100**, 5407-5412.
38. A. T. Hoye, J. E. Davoren, P. Wipf, M. P. Fink and V. E. Kagan, *Acc. Chem. Res.*, 2008, **41**, 87-97.
39. B. C. Dickinson and C. J. Chang, *J. Am. Chem. Soc.*, 2008, **130**, 9638-9639.
40. S. Marrache and S. Dhar, *Proc. Natl. Acad. Sci. U. S. A.*, 2013, **110**, 9445-9450.
41. S. K. Bae, C. H. Heo, D. J. Choi, D. Sen, E.-H. Joe, B. R. Cho and H. M. Kim, *J. Am. Chem. Soc.*, 2013, **135**, 9915-9923.
42. R. K. Pathak, S. Marrache, D. A. Harn and S. Dhar, *ACS Chem. Biol.*, 2014, **9**, 1178-1187.
43. D.-L. Ma, D. S.-H. Chan and C.-H. Leung, *Acc. Chem. Res.*, 2014.
44. J. Rejman, V. Oberle, I. Zuhorn and D. Hoekstra, *Biochem. J.*, 2004, **377**, 159-169.
45. J. P. Richard, K. Melikov, H. Brooks, P. Prevot, B. Lebleu and L. V. Chernomordik, *J. Biol. Chem.*, 2005, **280**, 15300-15306.
46. E. Blanchard, S. Belouzard, L. Goueslain, T. Wakita, J. Dubuisson, C. Wychowski and Y. Rouillé, *J. Virol.*, 2006, **80**, 6964-6972.
47. I. R. Nabi and P. U. Le, *J. Cell Biol.*, 2003, **161**, 673-677.
48. J. Rejman, A. Bragonzi and M. Conese, *Mol. Ther.*, 2005, **12**, 468-474.
49. J. S. Wadia, R. V. Stan and S. F. Dowdy, *Nat. Med.*, 2004, **10**, 310-315.
50. I. M. Kaplan, J. S. Wadia and S. F. Dowdy, *J. Controlled Release*, 2005, **102**, 247-253.
51. C. A. Puckett, R. J. Ernst and J. K. Barton, *Dalton Trans.*, 2010, **39**, 1159-1170.
52. S.-F. Peng, M. T. Tseng, Y.-C. Hoc, M.-C. Wei, Z.-X. Liao and H.-W. Sung, *Biomaterials*, 2011, **32**, 239-248.
53. F. Madani, S. Lindberg, Ü. Langel, S. Futaki and A. Gräslund, *J. Biophys.*, 2011, **2011**, 1-10.
54. R. G. W. Anderson, *Annu. Rev. Biochem.*, 1998, **67**, 199-225.
55. S. Trabulo, A. L. Cardoso, M. Mano and M. C. P. De Lima, *Pharmaceuticals*, 2010, **3**, 961-993.
56. K. Minezaki, M. Suleiman and R. Chapman, *J. Physiol.*, 1994, **476**, 459-471.
57. I. G. Zigoneanu, Y. J. Yang, A. S. Krois, M. E. Haque and G. J. Pielak, *BBA-Biomembranes*, 2012, **1818**, 512-519.
58. D. M. Cohen and E. Fisher, *J. Chem. Soc.*, 1962, 3044-3052.
59. J. Brynestad and G. P. Smith, *J. Phys. Chem.*, 1968, **72**, 296-300.
60. G. Consiglio, S. Failla, P. Finocchiaro, I. P. Oliveri and S. D. Bella, *Dalton. Trans.*, 2012, **41**, 387-395.
61. O. Jurček, M. Cametti, M. Pontini, E. Kolehmainen and K. Rissanen, *Org. Biomol. Chem.*, 2013, **11**, 4585-4590.
62. I. P. Oliveri, G. Maccarrone and S. Di Bella, *J. Org. Chem.*, 2011, **76**, 8879-8884.
63. S. Davis, M. Weiss, J. Wong, T. J. Lampidis and L. B. Chen, *J. Biol. Chem.*, 1985, **260**, 13844-13850.
64. D. Piwnica-Worms, J. F. Kronauge and M. L. Chiu, *Circulation*, 1990, **82**, 1826-1838.
65. M. L. Chiu, J. F. Kronauge and D. Piwnica-Worms, *J. Nucl. Med.*, 1990, **31**, 1646-1653.
66. A. C. Komor and J. K. Barton, *Chem. Commun.*, 2013, **49**, 3617-3630.
67. C. A. Puckett and J. K. Barton, *Biochemistry*, 2008, **47**, 11711-11716.
68. J. Wang, J. D. Byrne, M. E. Napier and J. M. DeSimone, *Small*, 2011, **7**, 1919-1931.
69. E. E. Bellocchio, R. J. Reimer, R. T. Fremeau and R. H. Edwards, *Science*, 2000, **289**, 957-960.

